Synthesis of sandwich microstructured expanded graphite/barium ferrite connected with carbon nanotube composite and its electromagnetic wave absorbing properties

Zhao, Tingkai; Jin, Wenbo; Ji, Xianglin; Jiang, Yuting; Dong, Ying; Yang, Yali; Dang, Alei; Li, Hao; Li, Tiehu; Shang, Songmin; Zhou, Zhongfu

Published in:
Journal of Alloys and Compounds

DOI:
10.1016/j.jallcom.2017.04.070

Publication date:
2017

Citation for published version (APA):
Zhao, T., Jin, W., Ji, X., Jiang, Y., Dong, Y., Yang, Y., Dang, A., Li, H., Li, T., Shang, S., & Zhou, Z. (2017). Synthesis of sandwich microstructured expanded graphite/barium ferrite connected with carbon nanotube composite and its electromagnetic wave absorbing properties. *Journal of Alloys and Compounds*, *712*, 59-68. https://doi.org/10.1016/j.jallcom.2017.04.070

Accepted Manuscript

Synthesis of sandwich microstructured expanded graphite/barium ferrite connected with carbon nanotube composite and its electromagnetic wave absorbing properties

Tingkai Zhao, Wenbo Jin, Xianglin Ji, Huibo Yan, Yuting Jiang, Ying Dong, Yali Yang, Alei Dang, Hao Li, Tiehu Li, Songmin Shang, Zhongfu Zhou

PII: S0925-8388(17)31261-6

DOI: 10.1016/j.jallcom.2017.04.070

Reference: JALCOM 41474

To appear in: *Journal of Alloys and Compounds*

Received Date: 25 January 2017

Revised Date: 29 March 2017

Accepted Date: 7 April 2017

Please cite this article as: T. Zhao, W. Jin, X. Ji, H. Yan, Y. Jiang, Y. Dong, Y. Yang, A. Dang, H. Li, T. Li, S. Shang, Z. Zhou, Synthesis of sandwich microstructured expanded graphite/barium ferrite connected with carbon nanotube composite and its electromagnetic wave absorbing properties, *Journal of Alloys and Compounds* (2017), doi: 10.1016/j.jallcom.2017.04.070.

Graphical abstracts

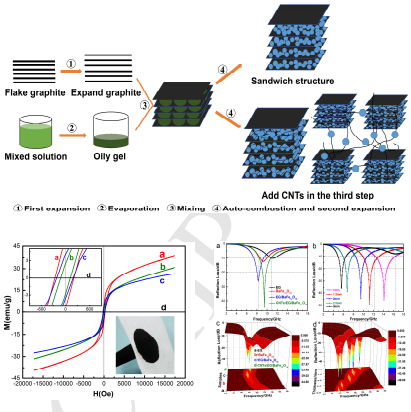

The sandwich microstructured expand graphite (EG)/$BaFe_{12}O_{19}$ (BF) nanocomposite successfully prepared by *in-situ* sol-gel auto-combustion method, the sandwich microstructured EG/BF connected with carbon nanotubes (CNTs) can further improve the electromagnetic performance effectively. The maximum reflection loss of the sandwich microstructured CNT/EG/BF composites with a thickness of 1 mm was up to -45.8 dB and the frequency bandwidth below -10 dB could reach to 4.2 GHz within the frequency range of 2-18 GHz.

Synthesis of sandwich microstructured expanded graphite/ barium ferrite connected with carbon nanotube composite and its electromagnetic wave absorbing properties

Tingkai Zhao[a,*], Wenbo Jin[a,*], Xianglin Ji[a], Huibo Yan[a], Yuting Jiang[a], Ying Dong[a], Yali Yang[a], Alei Dang[a], Hao Li[a], Tiehu Li[a], Songmin Shang[b], Zhongfu Zhou[c]

[a] *State Key Laboratory of Solidification Processing, Shaanxi Engineering Laboratory for Graphene New Carbon Materials and Applications, School of Materials Science and Engineering, Northwestern Polytechnical University, Xi'an 710072, China*

[b] *Institute of Textiles and Clothing, The Hong Kong Polytechnic University, Kowloon, Hong Kong*

[c] *Department of Physics, Aberystwyth University, Aberystwyth SY23 3FL, UK*

Abstract: The pursuing aim of high reflection loss and broad frequency bandwidth for electromagnetic wave (EMW) absorbing materials is a long-term task and under a close scrutiny. To construct rational microstructures for the absorber have significant impacts on increasing reflection loss and broadening frequency bandwidth. Herein, we presented a sandwich microstructured expand graphite (EG)/$BaFe_{12}O_{19}$ (BF) nanocomposite successfully prepared by *in-situ* sol-gel auto-combustion method. The experimental results showed that EG/BF nanocomposite has better EMW absorbing performance than pure EG and BF, the sandwich microstructured EG/BF connected with carbon nanotubes (CNTs) could further improve the electromagnetic performance effectively. The obtained CNT/EG/BF nanocomposite exhibited a saturation magnetization of 26.5 $emu \cdot g^{-1}$ at room temperature and an excellent EMW absorbing

* Corresponding Authors email: ztk-xjtu@163.com (Zhao TK) and wenbo_jin@126.com (Jin WB)

performance. The maximum reflection loss of the sandwich microstructured CNT/EG/BF composites with a thickness of 1 mm was up to -45.8 dB and the frequency bandwidth below -10 dB could reach to 4.2 GHz within the frequency range of 2-18 GHz. The research results indicated that the prepared nanocomposite showed great potential as a new type of microwave absorbing material.

Keywords: expanded graphite; $BaFe_{12}O_{19}$; carbon nanotube; sol-gel auto-combustion; sandwich microstructure; electromagnetic wave absorbing property

1. Introduction

Electromagnetic wave (EMW) absorbing materials have attracted great technical and scientific interests due to their extensive applications in military, civilian areas and so on. With the development of radar technology, stealth aircraft, armor and warship show a strong viability and the invisibility of military equipment puts forward higher requirements on the microwave absorbing materials.[1,2] In addition, in recent years people have witnessed the serious problem of electromagnetic interference due to the multiplication of electronic products and devices in wireless communication tools, local area networks and other communication equipments.[3,4] To solve the electromagnetic interference problem, considerable interest has been attracted to EMW absorbing materials with higher efficiency and wider bandwidth. For a high performance EMW absorbing material, excellent dielectric loss and magnetic loss are two important technical requirements.[5] Especially, carbon materials such as graphite, graphene, expanded graphite (EG), single- or multi-walled carbon nanotubes (SWCNTs, MWCNTs), carbon fibers, conducting polymers have been widely used as EMW absorbing materials due to their lightweight, high conductivity, high stability and good dielectric properties.[6-9] Metal materials such as nickel,

iron, cobalt and their oxides and carbonyl iron powder have good magnetism performance and show good magnetic loss than carbon materials.[10-12] However, metal materials have disadvantages, such as heavy weight, poor corrosion resistance and oxidation resistance, which make these materials unsuitable for aircrafts, missile and some special areas. In order to obtain outstanding EMW absorbing performance, carbon and metal composites have attracted significant attention.[13-16]

EG is a kind of graphite compound with low density, large surface, anti-high temperature, oil absorption and excellent electrical conductivity, and it is easy to prepare in low cost. Generally, the graphite sheet spacing of EG is large and up to 1 μm, and it is conducive to the multiple reflection of EMW so that it could increase the EMW absorption loss.[17] EG is a traditional EMW absorbing materials and widely used as a millimeter wave absorbing material with excellent dielectric properties but low magnetic loss. EG which compounded with some magnetic loss materials, such as magnetic metal powder, ferrite material and other oxides, could improve the electromagnetic performance.[18,19] The ferrite is a mature EMW absorber, which has attractive magnetic properties, high magnetic loss, high Curie temperature, excellent chemical stability and low cost. Barium ferrite ($BaFe_{12}O_{19}$, BF) is one of the most versatile hard magnetic material, especially suitable for low-frequency applications with high magnetic coercivity, high electrical resistivity, low eddy current loss and excellent chemical stability, and it has been widely used in the field of EMW absorption.[20] Chen et al.[21] reported that EG/$CoFe_2O_4$ composite was prepared by co-precipitation method. In metal salt solution, the metal oxides are precipitated on the surface of the EG. However, this method is inefficient, and it is difficult to control the metal oxides proportion of the composite. Gairola et al.[22] studied barium ferrite/graphite/polyaniline

composites as electromagnetic shielding materials. The EG and barium ferrite were prepared separately, and then EG and barium ferrite mixed in polyaniline precursor solution. The mixture was polymerized and dried to obtain barium ferrite/graphite/polyaniline composites. The method is a simple physical mixing, and the EG and barium ferrite were distributed unevenly. Nowadays, there are several methods available to synthesize $BaFe_{12}O_{19}$ including co-precipitation, ball milling, hydrothermal treatment, auto-combustion method. Typically, sol-gel auto-combustion is a simple, safe and rapid synthesis process. It has many advantages such as energy-saving and time-saving, controllable process and reactants mixed evenly. A certain proportion of metal salt solution containing organic fuel is heated to form oily gel, and the oily gel precursor burns and maintains until the reaction is complete. The process contains an exothermic and self-sustaining chemical reaction between the metal salts gel and a suitable organic fuel. The heat which is necessary to drive the process is primarily provided by the exothermic reaction. Then the product is calcined at high temperature to obtain $BaFe_{12}O_{19}$.[23,24] Furthermore, it is worth noting that the sol-gel auto-combustion precursor of $BaFe_{12}O_{19}$ is oily gel and EG has large sheet spacing and oil absorption properties,[25] which provide a way to prepare sandwich microstructured EG/BF nanocomposite. When the oily gel forms $BFe_{12}O_{19}$, the volume increases rapidly and the secondary expansion of EG would take place. However, to our knowledge, the preparation and EMW absorbing properties of the sandwich microstructured EG/BF nanocomposite has not been reported previously.

Herein, the sandwich microstructured EG/BF nanocomposite was successfully prepared through *in-situ* sol-gel auto-combustion method. The EG/BF nnaocomposite significantly enhanced EMW absorbing performance compared to pure EG and pure $BaFe_{12}O_{19}$. To obtain

excellent EMW absorbing performance, CNTs were added to the sandwich microstructured EG/BF nanocomposite to improve its dielectric constant. The addition of CNTs made the separated sandwich EG/BF interconnected and formed a three-dimensional conductive network, and it was benefit to electrical conductivity of the nanocomposite and increase dielectric performance.[26,27]

2. Experimental section

2.1 Preparation of EG

EG was prepared through the rapid expansion of natural flake graphite intercalated compound at 800□. First, the natural flake graphite which was mixed with the mixture of H_2SO_4 and HNO_3 was stirred at room temperature for 1 hour. Then added $KMnO_4$ to the mixture and kept stirring for 2 hours. The products were washed several times with deionized water until pH=7 and dried them in a vacuum oven to form graphite intercalated compound. Final, the graphite intercalated compound was rapidly expanded at 800℃ to obtain EG.[28] The oxygen-containing groups intercalated between graphite sheet layers instantly decomposed into gas at high temperatures, and the spacing of graphite sheet layers and atomic layers were expanded.

2.2 In-situ synthesis of sandwich microstructured EG/BFand CNT/EG/BF nnaocomposite

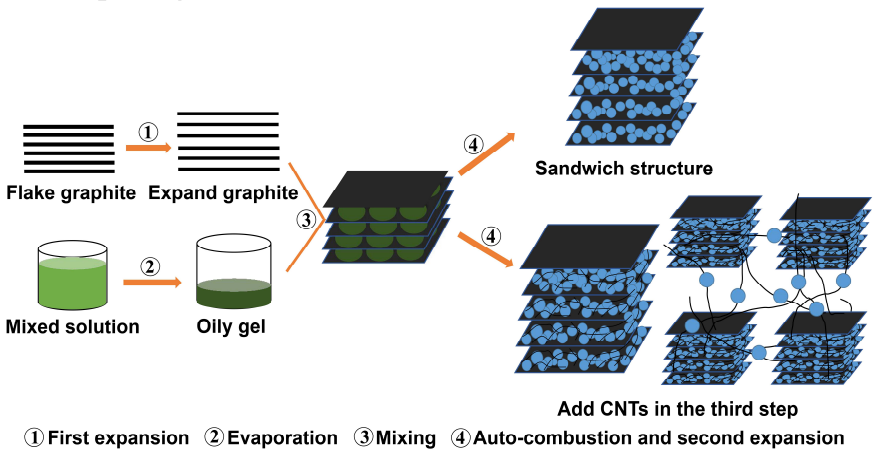

Fig. 1 The synthesis schematic diagram of sandwich microstructured EG/BF and CNT/EG/BF nanocomposite

The sandwich microstructured EG/BF nanocomposites were synthesized by *in-situ* sol-gel auto-combustion method and the schematic diagram is shown in Fig. 1. A certain amount of $Fe(NO)_3 \cdot 9H_2O$ and $Ba(NO)_2$ and citric acid were used as raw materials. First, $Fe(NO)_3 \cdot 9H_2O$ and $Ba(NO)_2$ were dissolved in deionized water and the mole ratio of Fe^{3+} to Ba^{2+} is 12:1. The citric acid was dissolved into the aqueous solution, and then mixed with the nitrate solution acquired above. The mole ratio of citric acid to total moles of Fe^{3+} and Ba^{2+} was fixed at 2:1. Ammonia solution was slowly added to the mixed solution until pH=7. The mixture was placed into a water bath at 80℃ for 3 hours and then the temperature was increased to 120℃ to evaporate water. The as-prepared EG was added in the oily gel with continuous stirring and the mass fraction of EG in the EG/BF composite is 15wt%. The temperature was increased to 200℃, the mixture bubbled up and automatically ignited. After the auto-combustion reaction, fluffy black block was obtained. Finally, the fluffy black block was calcined at 800℃ for 3 hours to obtain the sandwich microstructured EG/BF composite.[29] The type of CNTs is MWCNTs with an average diameter of about 8 nm and a length of 10-30 μm. Similarly, the CNT/EG/$BaFe_{12}O_{19}$ sandwich structured nanocomposite was obtained by simultaneously adding CNTs in the synthesis process of EG/BF composite, and the mass fraction of CNTs is 3wt%. The mass fraction of EG in CNT/EG/BF composite is also 15 wt% and the final proportion of the CNT/EG in CNT/EG/BF composites was 18 wt%.

2.3 Structural characterizations and microwave absorption measurements

For EMW parameter measurements, these different composites were uniformly mixed with 75 wt.% paraffin, and the mixtures were poured into the planar rectangular mold and dried about 24 hours in air. The prepared films were tailored precisely to the size of a rectangular waveguide

(22.86 mm ×10.16 mm) for EMW parameters test.

The morphology and microstructure of these nanocomposites were characterized using scanning electron microscope (SEM, FEINNS450, FEI) containing energy dispersive spectrometer (EDS) and transmission electron microscope (TEM, JEM-100CX11, FEI). Raman spectra of samples were measured using a Lab RAM HR confocal Raman system with 532 nm diode laser excitation at room temperature. X-ray diffraction (XRD, X'Pert Pro, PANalytical; with CuK_{α} radiation) patterns were performed to identify the phase structure. The hysteretic loops of samples were measured using Vibrating Sample Magnetometer (VSM, Lake Shore 7410, Quantum Design). The reflection loss of these nanocomposites was measured by a vector network analyzer (VNA Agilent technologies E8362B; 10 MHz-20 GHz).

3. Results and discussion

3.1 Morphological characterization

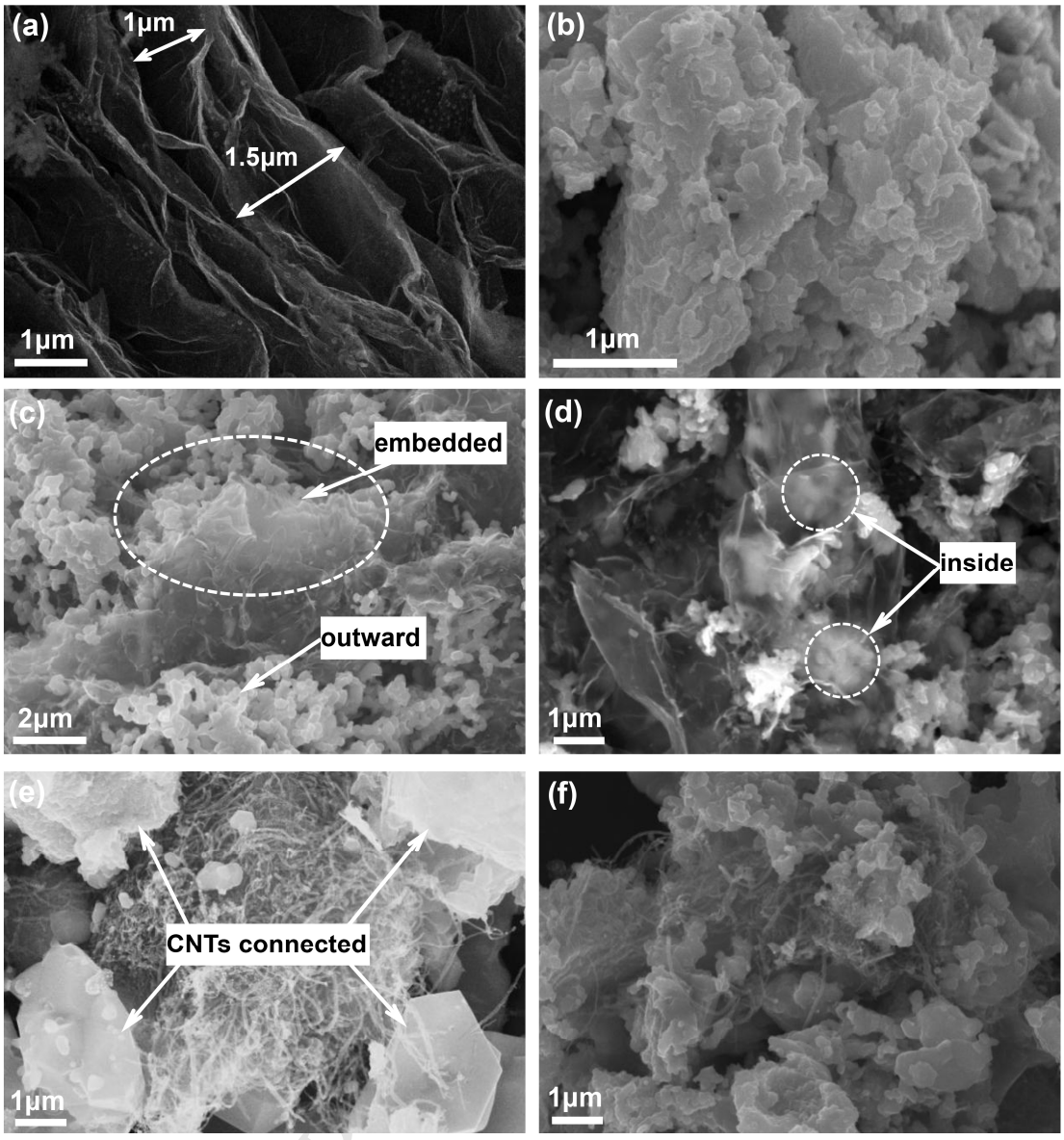

Fig. 2 SEM images of (a) EG (b) $BaFe_{12}O_{19}$, (c) and (d) EG/BF, (e) and (f) CNT/EG/BF nanocomposite

The SEM images of EG, BF, EG/BF and CNT/EG/BF nanocomposites are shown in Fig. 2. It exhibited the microstructure of EG and EG/BF composite. In Fig. 2(a), the microstructure of EG sheets can be clearly seen. The sheet spacing was up to 1.5 μm and each sheet consists of many graphene sheets. It should also be noted that the surfaces of the graphite sheets clearly exist some folds. Fig.2(b) shows the morphology of $BaFe_{12}O_{19}$. The particle sizes of $BaFe_{12}O_{19}$ are different and the mean diameter is about 100 nm. The sandwich microstructured EG/BF composite can be

seen in Fig. 2(c). The $BaFe_{12}O_{19}$ is embedded in the gap between graphite layers as shown in the labeling area, and it also can be found that some of $BaFe_{12}O_{19}$ particles are on the outside of the graphite sheets surface. The graphite sheets and $BaFe_{12}O_{19}$ particles can be clearly identified. Fig. 2(d) shows that the $BaFe_{12}O_{19}$ particles are wrapped with wrinkled graphite sheets and form sandwich microstructures. The graphite sheet is so thin that it appears to be translucent. In addition, it can be clearly seen that $BaFe_{12}O_{19}$ particles is sandwiched between the thin layers of graphite sheets as shown in the labeling area. Fig. 2(e) is the CNT/EG/BF nanocomposite. The four separated EG/BF components are connected with CNTs and form three-dimensional conductive networks. It is very important that the surface of CNTs was not smooth and they attached some $BaFe_{12}O_{19}$ particles indicating that CNTs also connect the $BaFe_{12}O_{19}$ particles. It is obvious to see that some $BaFe_{12}O_{19}$ particles are connected with CNTs in Fig. 2(f). CNTs went through the $BaFe_{12}O_{19}$ particles and connected them as a whole block. It is benefit to improve electrical conductivity of the nanocomposite.

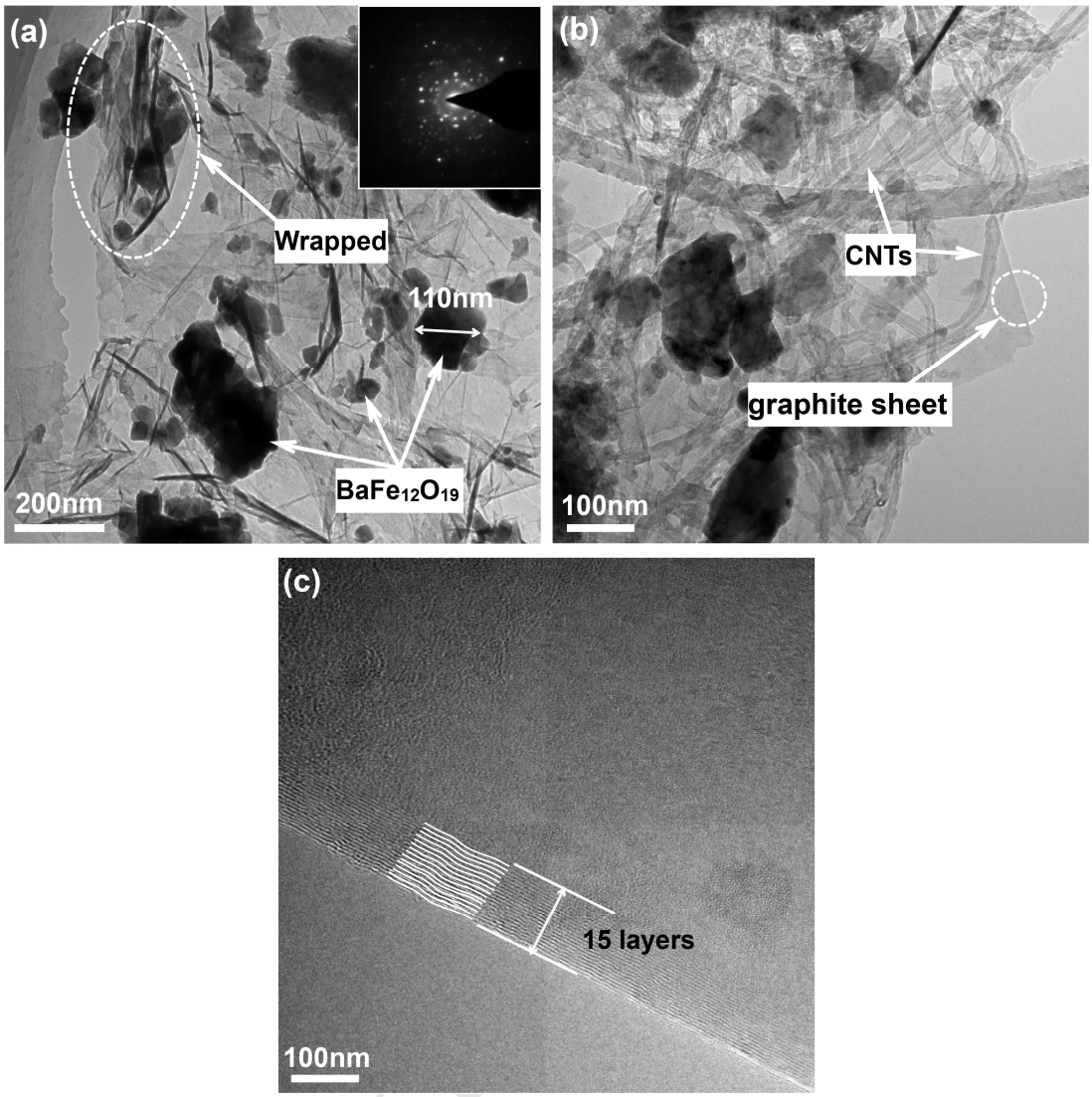

Fig. 3 TEM images of (a) EG/BF and (b)-(c) CNT/EG/BF nanocomposite

The TEM images of EG/BF and CNT/EG/BF composites are shown in Fig. 3. It is obvious to see that the graphite sheets with a lot of folds are very thin and showed a translucent film in Fig. 3(a). $BaFe_{12}O_{19}$ particles with various sizes distributed on the surface of graphite sheets and the mean diameter of these particles is about 110 nm. The electron diffraction pattern on the upper right corner indicates that the $BaFe_{12}O_{19}$ particles are not pure single crystal. In addition, the particles are irregularly shaped. According to the relevant literatures,[30,31] crystal shapes are related to crystal types, and different types may have different chemical contents. It is mainly duo

to the fact that the obtained $BaFe_{12}O_{19}$ particles is not pure single crystal, and the chemical contents for different crystal is different.

It should be noted that some $BaFe_{12}O_{19}$ particles are wrapped with graphite sheets as shown in the labeling area of the image and other $BaFe_{12}O_{19}$ particles was sandwiched between the thin transparent graphite sheets. Fig. 3(b) is the image of CNT/EG/BF nanocomposite. CNTs are intertwined and connected with the $BaFe_{12}O_{19}$ particles and graphite sheets. It is clear to see a piece of thin graphite sheet is embedded with the CNTs and $BaFe_{12}O_{19}$ particles and it shows a transparent film. Moreover, there are some other transparent graphite sheets and a portion of $BaFe_{12}O_{19}$ particles. Fig. 3(c) is high magnification TEM image of the circle area in Fig. 3(b). The thin graphite sheets have 15 layers, and it means that the secondary expansion of EG during the auto-combustion process of $BaFe_{12}O_{19}$ is adequate.

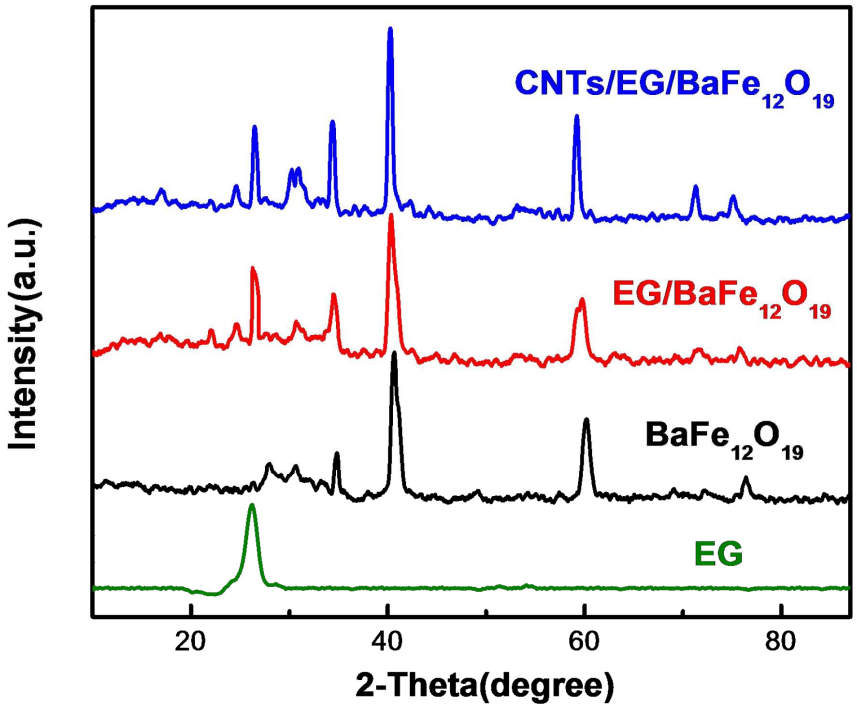

Fig. 4 XRD patterns of EG, BF, EG/BF and CNT/EG/BF composites

Fig. 4 shows the XRD patterns of EG, BF, EG/BF, and CNT/EG/BF composites. The characteristic diffraction peak of EG at 2θ=26.20° is corresponding to the d_{002} planes of graphite, indicating that the interlayer distance between two graphene layers is about 0.334 nm.[32] The main diffraction peaks of $BaFe_{12}O_{19}$ are observed at 2θ values of 31.36°, 33.22°, 35.16°, 38.12°, 41.32°, 43.46°, 50.68°, 56.08°, 57.54°, 59.08°, 69.65° and 76.32° corresponding to the (110), (107), (114), (108), (203), (205), (209), (217), (2011), (3011) (1022) and (220) lattice faces.[33,34] All the observed peaks of $BaFe_{12}O_{19}$ have been well matched with the standard XRD patterns which indicates that the $BaFe_{12}O_{19}$ was successfully achieved by sol-gel auto-combustion method. It can also be found that the XRD pattern of EG/BF nanocomposite is similar to that of $BaFe_{12}O_{19}$, and the EG/BF nanocomposite has a significant peak at about 26.20° compared to pure $BaFe_{12}O_{19}$. In addition, EG has a characteristic peak at 26.20° which indicating that no chemical reaction occurred between $BaFe_{12}O_{19}$ and EG. Furthermore, it should note that the displacement of (002) peak of graphite for EG/BF and CNT/EG/BF became narrower than pure EG. This may be due to the decomposition of the residual oxygen-containing groups of EG during the high-temperature roasting process, and it is benefit to the crystal structure of graphite.[35] Moreover, the relative intensity of (114) and (203) diffraction peaks in these composites have been changed as comparison with pure $BaFe_{12}O_{19}$, and this may be related with the crystal type and structure of the obtained $BaFe_{12}O_{19}$. It is due to the addition of EG and CNT affected the formation of $BaFe_{12}O_{19}$ and the crystal type and structure of $BaFe_{12}O_{19}$ maybe changed.[36] The XRD pattern of CNT/EG/BF nanocomposite has no significant difference with EG/BF nanocomposite due to the fact that characteristic peaks of CNTs are similar with graphite.

The size of $BaFe_{12}O_{19}$ particles was calculated using Debye-Schemer formula: $D = k\lambda/\beta cos\theta$,

where D is the average crystal size of particles, k is the shape factor, λ is the X-ray wavelength, θ is the half angle in degrees and β is the full width at half maximum. *k* is often assigned a value of 0.89, which depends on several factors, including the Miller index of the reflecting plane and the shape of the crystal.[37] The (205) reflection of the observed X-ray data is chosen for calculating the size of $BaFe_{12}O_{19}$ particles. The average size of the $BaFe_{12}O_{19}$ particles calculated using the above mentioned equation was estimated about 106 nm, and it is in excellent agreement with the mean particle size determined by TEM.

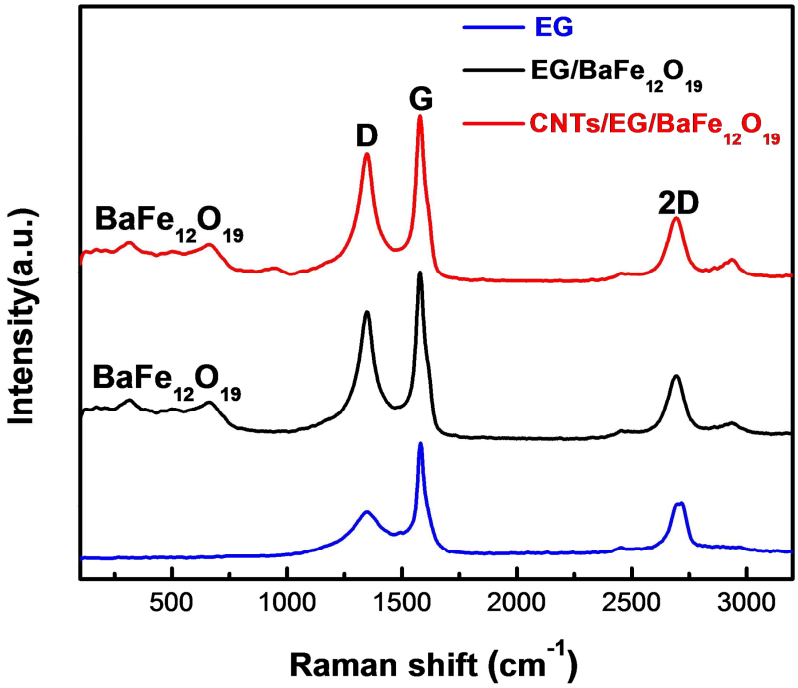

Fig. 5 Raman spectra of EG, EG/BF and CNT/EG/BF composites

Raman spectrum is an important and useful tool for characterizing carbon materials. Fig. 5 shows the Raman spectra of EG, EG/BF and CNT/EG/BF composites. The Raman spectrum of EG showed the characteristic D, G and 2D bands at 1350 cm^{-1}, 1580 cm^{-1} and 2680 cm^{-1} respectively. G band is associated with E_{2g} symmetry, and it is generated due to the in-plane vibration of the sp^2 carbon atoms of graphite. D band appears from a breathing mode of *K*-point phonons of A_{1g}

symmetry and it implies the degree of graphite defects and irregularities.[38] 2D peak originates from the double-resonance Raman process of two phonons with opposite momentum. The intensity ratio of D and G peaks (I_D/I_G) has been used as estimation for the degree of ordered and disordered structures in graphite sheets.[39,40] It can be seen that the Raman spectrum of EG/BF nanocomposite is significantly different from EG. The 2D peak had no obvious change, whereas the D peak had a visible increase. The increased I_D/I_G value indicates that the degree of disorder structure in the graphite sheet increased. It is because the auto-combustion process of ferrite oily gel precursor made EG peeled into thin graphite sheets and it has a certain degree of damage to the microstructure of the graphite sheets. In addition, there are some ferrite peaks between 260 cm^{-1} and 700 cm^{-1}, and it shows the Raman spectrum of $BaFe_{12}O_{19}$. The Raman spectrum of CNT/EG/BF composite is almost the same as EG/BF composite. However, according to the relevant data, the CNTs have a characteristic peak at about 160 cm^{-1}.[41] And the reason for this phenomenon is that the proportion of CNTs is small and the characteristic peak at 160 cm^{-1} may be mixed with $BaFe_{12}O_{19}$. Moreover, the peaks position of CNTs are close to EG sheets.[42] It is difficult to identify the peak of CNTs at160 cm^{-1}.

3.2 Magnetic properties

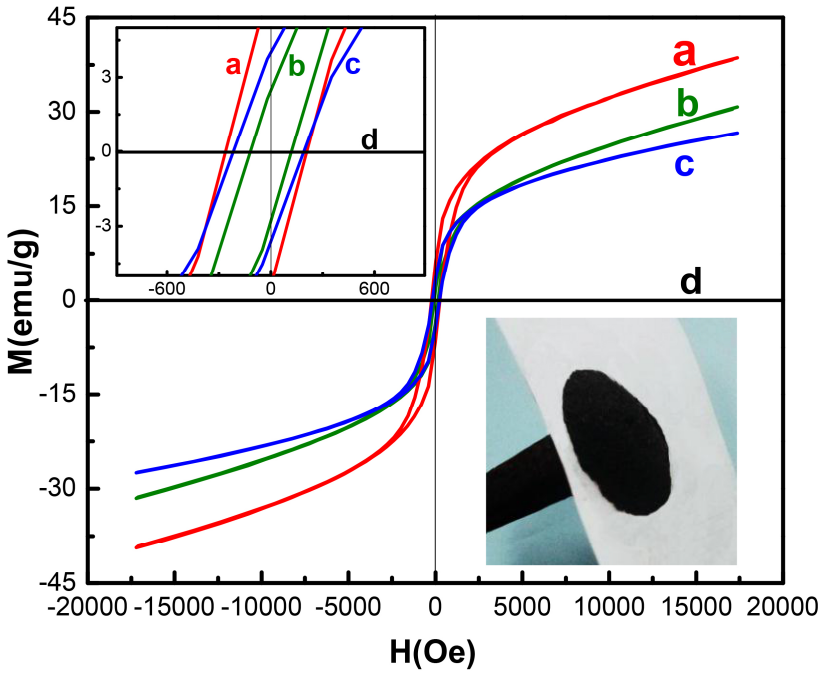

Fig. 6 Optical picture and the hysteretic loops of (a) $BaFe_{12}O_{19}$, (b) EG/BF, (c) CNT/EG/BF (d) EG

The hysteretic loops of BF, EG/BF, EG/BF connected with CNTs and pure EG were measured at room temperature and the experimental results are shown in Fig. 6. The saturation magnetization (M_S) value can be obtained from the M value as H goes to infinity, while coercivity (H_C) and the remanent magnetization values are directly obtained from the hysteretic loops. The M_S value of $BaFe_{12}O_{19}$ is found to be 38.5 emu·g^{-1} at an external field of 15 kOe. It can be found that the hysteretic loops of EG/BF and CNT/EG/BF composites are quite similar with the M_S values of 30.6 emu·g^{-1} and 26.5 emu·g^{-1} respectively, and these values are lower than pure $BaFe_{12}O_{19}$. From the published literature,[43] we can see that as the non-magnetic phase increases, the M_S value decreases, and the result of this work is very similar with that literature. With the addition of non-magnetic EG and CNTs, the corresponding M_S values reduced. This is due to the addition of EG and CNTs reduced the magnetic saturation strength. The high M_S values of the samples make them easy to be adsorbed by a magnet as shown in the picture at the lower right

corner of the Fig. 6. The hysteretic loops of EG indicates that the EG is nonmagnetic. It can also be seen from the enlarged image on the upper left corner that the coercivity of $BaFe_{12}O_{19}$, EG/BF and CNT/EG/BF composites is 213.5, 115.2 and 190.1 Oe respectively. The high coercivity is benefit to the magnetic loss at a relatively low frequency. The adding content of EG reduced the coercivity in contrast to pure $BaFe_{12}O_{19}$, because EG is nonmagnetic.[44] Also, it should be noted that the values of coercivity for EG/BF and EG/CNT/BF samples are significant different. The CNT/EG/BF shows higher value than EG/BF, and the possible reason is the connection function of CNTs affected the formation process of $BaFe_{12}O_{19}$ grain and the grain size of the $BaFe_{12}O_{19}$ may be changed. The coercive force is related to the grain size of $BaFe_{12}O_{19}$, thus the coercive force changed.[45]

3.3 Electromagnetic wave absorbing properties

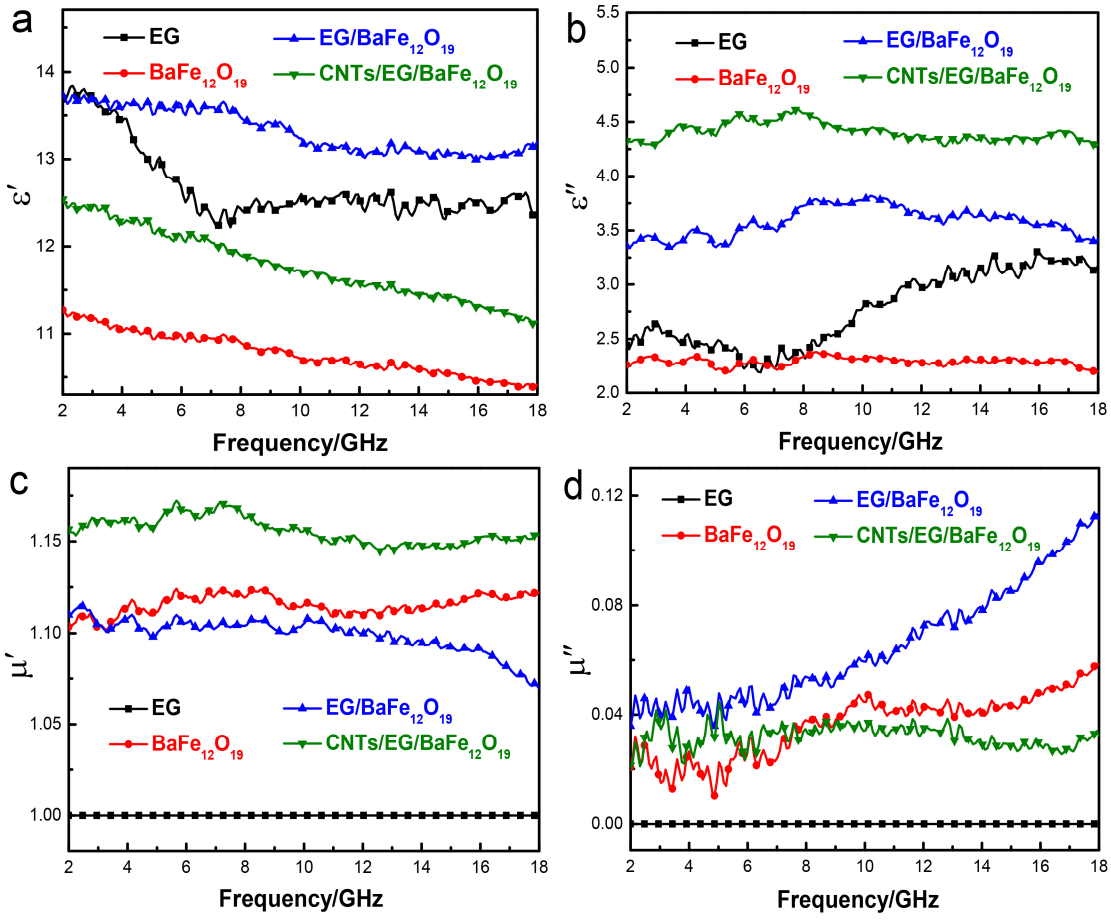

Fig. 7 Complex permittivity (ε′, ε") and complex permeability (μ′, μ") spectra of EG, BF, EG/BF and CNT/EG/BF *vs*. frequency within the frequency range of 2-18 GHz

The complex permittivity (ε′, ε") and permeability (μ′, μ") spectra of EG, BF, EG/BF and CNT/EG/BF *vs*. frequency within the frequency range of 2-18 GHz are shown in Fig. 7. The real part of complex permittivity and permeability are mainly associated with the amount of polarization occurring in the material and it symbolizes the storage ability of the electric and magnetic energy, whereas the imaginary part accounts for dielectric constant and magnetic loss, respectively.[46] The real part of complex permittivity spectra for different materials are shown in Fig. 7(a), and its values are related to the electric conductivity of these composites. The value of EG/BF is the highest while the pure $BaFe_{12}O_{19}$ is the lowest and the value of pure EG is lower than EG/BF. It is mainly because ferrite conductivity is poor and EG piece in the paraffin matrix dispersion spacing is relatively large. Moreover, the graphite sheets in EG/BF nanocomposite are very thin due to the secondary expansion of EG during the auto-combustion process. In addition, the value of EG/BF is higher than that of CNT/EG/BF. It may be related to the dispersion of the conductive phase in the paraffin matrix. CNTs has a significant connection function, which limit the dispersion of CNT/EG/BF in the matrix. EG/BF has good dispersion in paraffin matrix and CNT/EG/BF is poor. Thus the <epsilon>'EG/BF > <epsilon>'CNT/EG/BF.[47] The overall trend of the real part decreases with the frequency increasing and EG has a bit decline at 7.2 GHz. It can be found that the combination with EG effectively improved the real part of complex permittivity of $BaFe_{12}O_{19}$. The imaginary part of complex permittivity spectra for different materials are shown in Fig. 7(b). It should be noted that the value of $BaFe_{12}O_{19}$ and EG/BF are about 2.3 and 3.6 respectively while the CNT/EG/BF can reach to 4.5. The CNT/EG/BF nanocomposite shows

high dielectric constant owing to the CNTs connected the separated EG/BF into three-dimension conductive networks, which may enhance the conductivity and electric polarization of the nanocomposite.[48] Fig. 7(c) and Fig. 7(d) shows the complex permeability spectra for different materials. The real and imaginary parts of EG is 1 and 0 respectively, and it is owing to the fact that EG is non-magnetic. The spectra of real parts for $BaFe_{12}O_{19}$ and EG/BF are similar and the value of BF is a little bit high due to that EG is nonmagnetic. Their values are about 1.11 while the CNT/EG/BF nanocomposite value is about 1.14 showing good magnetic properties. The high complex permeability real part means better impedance matching and it benefits to the EMW absorption. The imaginary part of complex permeability is the estimation of magnetic loss. Magnetic materials generate magnetic losses during the repeated magnetization and demagnetization process in the electromagnetic field and the magnetic loss intensity is related to EMW frequency.[49] In Fig. 7(d), $BaFe_{12}O_{19}$ and CNT/EG/BF composite show similar spectra and they are steady compared to EG/BF, and the values are about 0.35 and 0.03, respectively. With the frequency increasing, the imaginary part of complex permeability of pure EG/BF increased, and it shows a higher value than CNT/EG/BF composite especially at high frequencies. It is mainly due to that the process cycle of magnetization and demagnetization increased at high frequencies and the added CNTs without magnetic loss have a certain proportion in the CNT/EG/BF nanocomposite. Moreover, it can be found that the frequency dependence of the imaginary part for EG/BF and EG/CNT/BF composites is different. This may be due to the fact that the addition of CNTs affected the microstructure of the composite and the grain size of $BaFe_{12}O_{19}$, because CNTs have significant connection function in the composite. The grain size and crystal structure of $BaFe_{12}O_{19}$ maybe changed the value of imaginary part.[50,51]

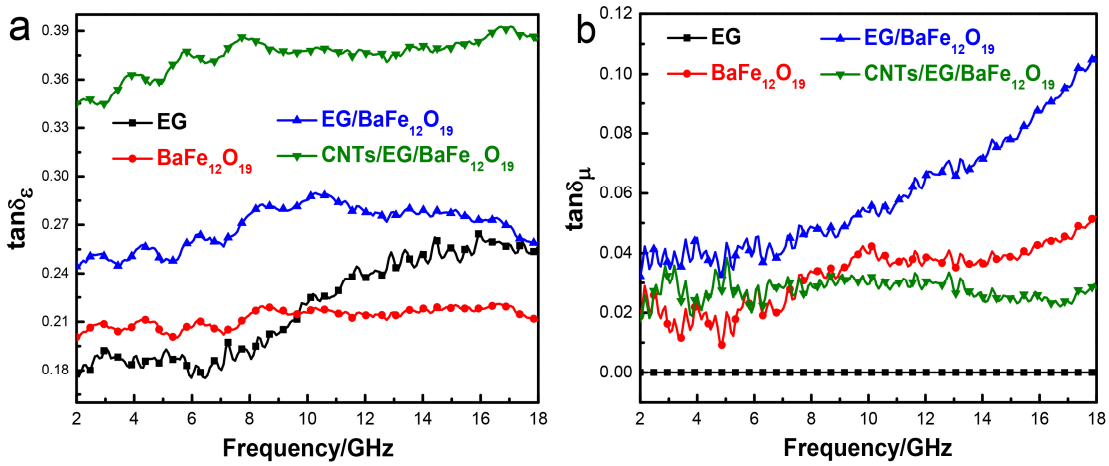

Fig. 8 The dielectric loss tangent ($tan\delta_\varepsilon$) and magnetic loss tangent ($tan\delta_\mu$) spectra of EG, BF, EG/BF and CNT/EG/BF *vs*. frequency within the frequency range of 2-18 GHz

The loss tangent is the estimation of electromagnetic loss capability for the absorbing material and generally a large loss tangent is expected. Fig. 8 shows the dielectric loss tangent ($tan\delta_\varepsilon=\varepsilon''/\varepsilon'$) and magnetic loss tangent ($tan\delta_\mu=\mu''/\mu'$) spectra of EG, $BaFe_{12}O_{19}$, EG/BF and CNT/EG/BF *vs*. frequency in 2-18 GHz. It should be noted that $tan\delta_\varepsilon$ is higher than $tan\delta_\mu$ for the same material regardless of the frequency which indicates that the reflection loss is mainly affected by the dielectric loss. The $tan\delta_\varepsilon$ of CNT/EG/BF shows the highest value and its average value is about 0.375 while the average value of pure EG/BF is only about 0.27 as shown in Fig. 8(a). The dielectric loss has a significant increase means that the CNT/EG/BF has more excellent EMW absorption performance than pure $BaFe_{12}O_{19}$ and it is owing to that CNTs connected with $BaFe_{12}O_{19}$ and the separated EG/BF components, and they formed three-dimensional conductive networks. The impedance matching of pure EG and the conductivity of pure $BaFe_{12}O_{19}$ are both poor which lead to the lower $tan\delta_\varepsilon$, and EG/BF shows a higher $tan\delta_\varepsilon$ due to the excellent electrical conductivity of EG. In Fig.8(b), $BaFe_{12}O_{19}$ and CNT/EG/BF show close spectra of $tan\delta_\mu$, whereas EG/BF is slightly high and the $tan\delta_\mu$ value increased with the frequency increasing. These values

of tanδ_μ are quite low indicating a weak magnetic loss.[52]

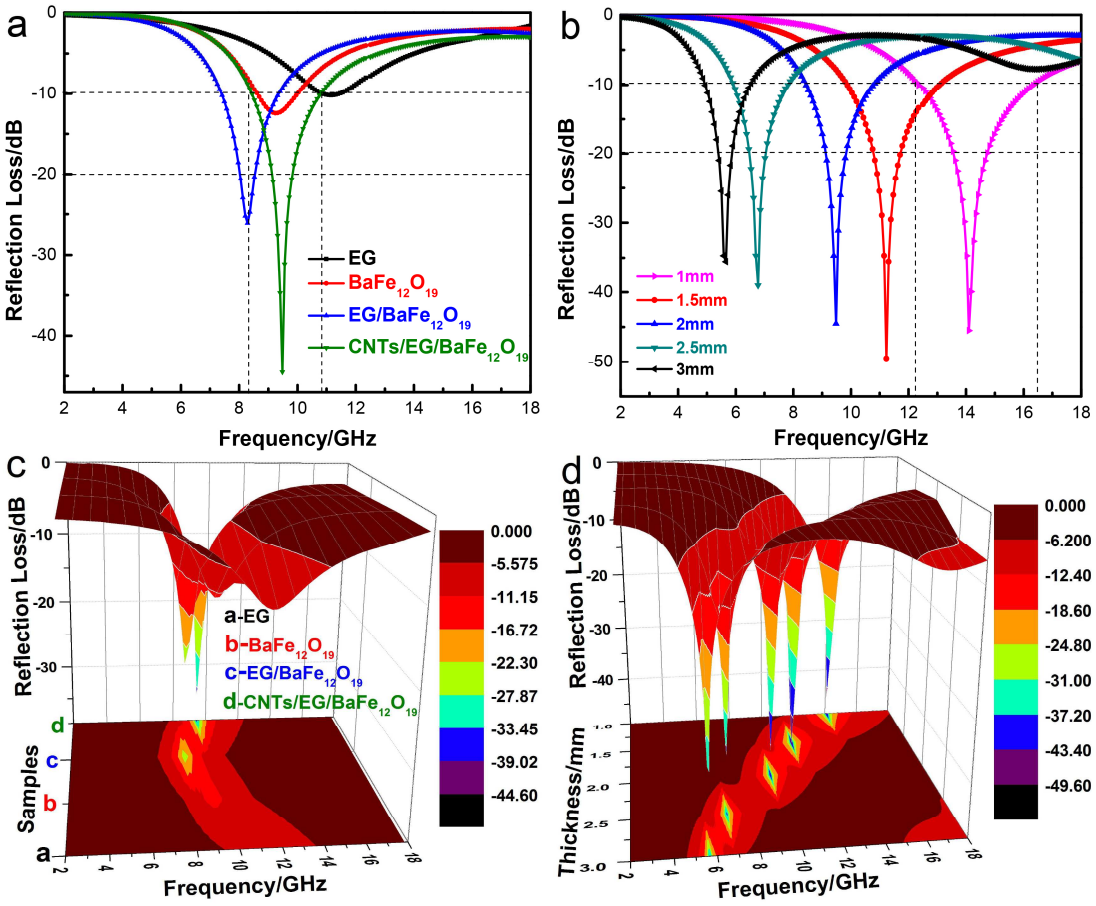

Fig. 9 (a) and (c) Reflection loss curves of EG, $BaFe_{12}O_{19}$, EG/BF and CNT/EG/BF *vs*. frequency in 2-18 GHz, (b) and (d) reflection loss curves of CNT/EG/BF nanocomposite with different thickness vs. frequency in 2-18 GHz

Table 1 The ferrite composites prepared by different methods and their properties

Authors	Composites	Range (dB)	Maximum reflection loss (dB)	Bandwidth (GHz)
Chen[17]	$EG/NiFe_2O_4$	< -10	-14.60	2.88
Wang[53]	$EG/CoFe_2$	< -10	-19.13	3.37
Hou[6]	$CNTs/Fe_3O_4$	< -10	-18.22	2.23
Sutradhar[54]	$CNTs/Ni_{0.4}Zn_{0.4}Cu_{0.2}Fe_2O_4$	< -10	-26.35	2.60
This work	$CNTs/EG/BaFe_{12}O_{19}$	< -10	-45.80	4.15

Table 1 shows the different ferrite composites and their properties. It can be easily found that the composites using this work exhibit good electromagnetic performance. The maximum reflection loss reach to -45.8 dB and the effective bandwidth can reach to 4.2 GHz. It means the sandwich microstructured composite has excellent EMW absorption performance.

For single-layer absorber, according to the transmission theory, the calculation formulas are given as follows:

$$R(dB) = 20 \log_{10} \left| \frac{Z_{in} - 1}{Z_{in} + 1} \right| \quad (1)$$

$$Z_{in} = \left(\frac{\mu_r}{\varepsilon_r} \right)^{\frac{1}{2}} \tanh \left[j \left(\frac{2\pi f d}{c} \right) (\mu_r \varepsilon_r)^{\frac{1}{2}} \right] \quad (2)$$

where Z_{in} is the normalized input impedance at the free space and material interface, $\varepsilon_r=\varepsilon-j\varepsilon''$ is the complex permittivity, $\mu_r=\mu'-j\mu''$ is the complex permeability of absorber, f is the frequency of the microwaves in free space, d is the thickness of the absorber, and c is the velocity of light in free space, respectively.[55] The reflection loss curves of different samples with the same thickness (2 mm) are shown in Fig. 9(a). As can be seen from this figure, the reflection loss curves of EG/BF and CNT/EG/BF exhibit two peaks with the maximum value of -26.1 dB at 8.2 GHz and -44.5 dB at 9.6 GHz respectively, and the value of reflection loss below -10 dB for CNT/EG/BF was up to 2.49 GHz. The CNTs increased the reflection loss due to their excellent electrical conductivity and three-dimensional web structures. In addition, it can be found that the reflection loss of pure EG and pure $BaFe_{12}O_{19}$ are quite low, indicating that the combination of EG and pure $BaFe_{12}O_{19}$ greatly improves the reflection loss. This is probably due to the fact that the dielectric loss of EG and the magnetic loss of $BaFe_{12}O_{19}$ are complementary. The three-dimensional picture of reflection loss for EG, $BaFe_{12}O_{19}$, EG/BF and the CNT/EG/BF is shown in Fig. 9(c), it is clear to

see that EG/BF shows better EMW absorption performance than EG and $BaFe_{12}O_{19}$, and the CNT/EG/BF is the best. The performance of the absorber mainly depends on two factors: the impedance matching of interface and the complementarity between dielectric constant and magnetic loss. For the good matching of impedance, a suitable electrical conductivity for the absorber is required. Both high and low conductivity results in bad microwave absorption due to the skin effect and poor current thermal effect, respectively.[56] The above results illustrate that CNT/EG/BF composite has good impedance matching and the complementarity between dielectric constant and magnetic loss. The schematic representation of EMW absorption mechanism of CNT/EG/BF nanocomposite is shown in Fig. 10.[57] The incident EMW has several kinds of interactions in the nanocomposite. The EMW has multiple reflections between graphite sheets and it increases the reflection loss. Moreover, the $BaFe_{12}O_{19}$ particles between graphite sheets can increase the magnetic loss effectively. The addition of CNTs could increase EMW transmission path and improve reflection loss.

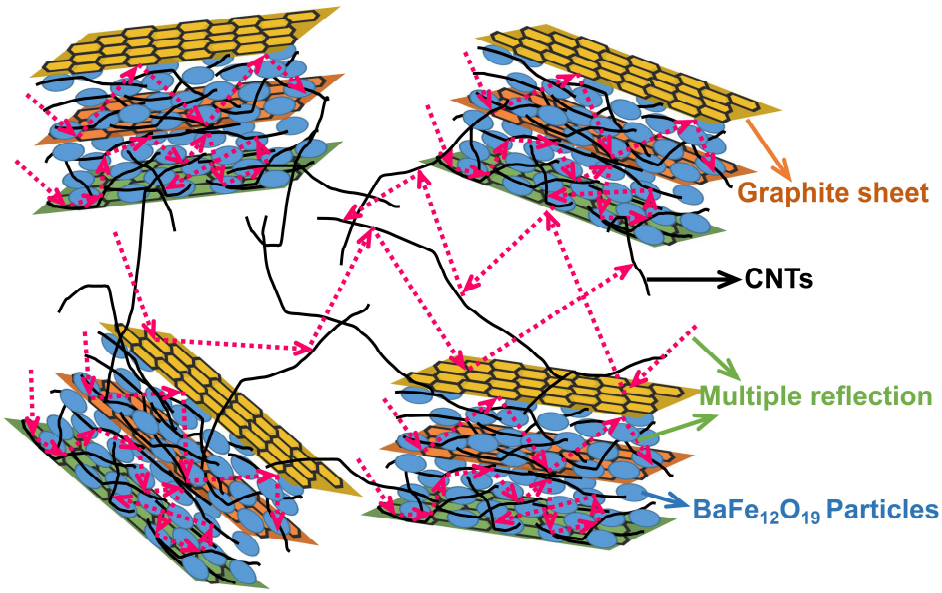

Fig. 10 Schematic representation of the EMW absorption mechanism in CNT/EG/BF nanocomposite

The CNT/EG/BF nanocomposite shows excellent EMW absorbing performance and in order

to determine the thickness effect on the EMW absorbing performance of the samples, the reflection loss of CNT/EG/BF nanocomposite with different thicknesses between 1-3 mm were calculated. The reflection loss curves are shown in Fig. 9(b) and the three-dimensional picture of reflection loss is shown in Fig. 9(d). It demonstrates that the maximum of reflection loss moves towards low frequency with the thickness increasing because of the different travel path and time of incident microwave in the absorber with different thickness and the synergistic effect of microwave absorption. The absorption frequency range could be adjusted by altering the thickness of samples according to the requirement.[58] For the potential absorbers, large bandwidth of absorption is expected. In this work, the sandwich microstructured CNT/EG/BF nanocomposite with a thickness of 1.5 mm shows the maximum reflection loss is up to -49.5 dB at 11.2 GHz, while the CNT/EG/BF with a thickness of 1 mm shows the maximum reflection loss could reach to -45.8 dB at 14.1 GHz as shown in Fig. 9(b). Moreover, it should be noted that the value of reflection loss below -10 dB is up to 4.2 GHz and below -20 dB could reach to 1.2 GHz with a thickness of 1 mm. The CNT/EG/BF nanocomposite exhibits excellent EMW absorbing properties and have potential applications.

4. Conclusions

In summary, the sandwich microstructured EG/BF nanocomposite was successfully prepared through *in-situ* sol-gel auto-combustion method. Compared to pure EG and $BaFe_{12}O_{19}$, the sandwich microstructured EG/BF nanocomposite showed good EMW absorbing properties. Furthermore, the sandwich microstructured EG/$BaFe_{12}O_{19}$ connected with CNTs nanocomposite could significantly improve their dielectric performance. The adding of CNTs made the separated sandwich microstructured EG/BF components interconnected and formed three-dimensional

conductive networks, and it was benefit to electrical conductivity of the nanocomposite and increase dielectric performance. The as-obtained CNT/EG/BF nanocomposite exhibited a saturation magnetization of 26.5 emu·g^{-1} at room temperature and has an excellent EMW absorbing performance. The maximum reflection loss CNT/EG/BF nanocomposite with a thickness of 1 mm was up to -45.8 dB and the frequency bandwidth below -10 dB could reach to 4.2 GHz within the frequency range of 2-18 GHz. The nanocomposite with excellent EMW absorbing performance and simple production process might find extensive applications in the fields of military, governance of electromagnetic pollution and so on.

Acknowledgments

This work was supported by the Natural Science Foundation of China (51572221, 51672221), the China Aeronautical Science Fund (2014ZF53074), the Natural Science Foundation of Shaanxi Province (2016JQ5108) and the Graduate Innovation Seed Fund of Northwestern Polytechnical University (Z20160011).

References

[1] L. Matzui, L. Vovchenko, Y. Prylutskyy, I. Korotash, V. Matzui, P. Eklund, U. Ritter, P. Scharff, Electromagnetic losses in carbon-epoxy composites, Mater. Sci. Eng. C 27 (2007) 1007-1009.

[2] L. Vovchenko, L. Matzui, V. Oliynyk, V. Launeit, Y. Prylutskyy, D. Hui, Y. M. Strzhemechny, Modified exfoliated graphite as a material for shielding against electromagnetic radiation, Int. J. Nanosci. 7 (2011) 263-268.

[3] B. Qu, C. Zhu, C. Li, X. Zhang, Y. Chen, Coupling hollow Fe_3O_4-Fe nanoparticles with graphene sheets for high-performance electromagnetic wave absorbing material, ACS

Appl. Mater. Interfaces 8 (2016) 6.

[4] P. Liu, Y. Huang, X. Zhang, Synthesis, characterization and excellent electromagnetic wave absorption properties of graphene/poly (3,4-Ethylenedioxythiophene) hybrid materials with Fe_3O_4 nanoparticles, J. Alloys Compd. 617 (2014) 511-517.

[5] G. Wan, J. Jiang, Y. He, S. Bie, Optimal design and loss mechanism analysis of microwave absorbing unidirectional SiC fiber composites with broad absorption band and good polarization stability, J. Appl. Phys. 119 (2016) 134906.

[6] T. K. Zhao, X.L. Ji, W.B. Jin, C.Y. Xiong, W.X. Ma, C. Wang, S.C. Duan, A.L. Dang, H. Li, T. H. Li, S.M. Shang, Z.F. Zhou, Synthesis and electromagnetic wave absorption property of amorphous carbon nanotube networks on a 3D graphene aerogel/$BaFe_{12}O_{19}$ nanocomposite, J. Alloys Compd. 708 (2017) 115-122.

[7] T. A. Len, Transport properties of composites with carbon nanotube-based composites, Fuller. Nanotub. Car. N. 13 (2005) 259-265.

[8] A. Lazarenko, L. Vovchenko, D. Matsui, Y. Prylutskyy, L. Matzuy, U. Ritter, P. Scharff, Electrical and thermal conductivity of polymer-nanocarbon composites, Mol. Cryst. Liq. Cryst. 497 (2008) 397-407.

[9] M. Melnichenko, Electrodynamic properties of the nanocarbon/polymer composites with aligned by magnetic field secondary non-conductive component, Proceedings of SPIE-The International Society for Optical Engineering 9519(2015) 223-233.

[10] Y. Huang, H. Zhang, G. Zeng, Z. Li, D. Zhang, H. Zhu, R. Xie, L. Zheng, J. Zhu, The microwave absorption properties of carbon-encapsulated nickel nanoparticles/silicone resin flexible absorbing material, J. Alloys Compd. 682 (2016) 138-143.

[11] C. Zhao, M. Shen, Z. Li, R. Sun, A. Xia, X, Liu, Green synthesis and enhanced microwave absorption property of reduced graphene oxide-$SrFe_{12}O_{19}$ nanocomposites, J. Alloys Compd. 689 (2016) 1037-1043.

[12] T. K. Zhao, C. L. Hou, H. Zhang, R. X. Zhu, S. F. She, J. Wang, T. H. Li, Z. Liu, B. Wei, Electromagnetic wave absorbing properties of amorphous carbon nanotubes, Sci. Rep. 4 (2014) 5619-5619.

[13] J. Kong, J. Liu, F. Wang, L. Luan, M. Itoh, K. I. Machida, Electromagnetic wave absorption properties of Fe_3O_4 octahedral nanocrystallines in gigahertz range, Appl. Phys. A 105 (2011)

351-354.

[14] A. Namai, M. Yoshikiyo, K. Yamada, S. Sakurai, T. Goto, T. Yoshida, T. Miyazaki, M. Nakajima, T. Suemoto, H. Tokoro, Hard magnetic ferrite with a gigantic coercivity and high frequency millimetre wave rotation, Nat. Commun. 3 (2012) 251-280.

[15] G. E. Grechnev, V. A. Desnenko, A. V. Fedorchenko, A. S. Panfilov, Y. A. Kolesnichenko, L. Y. Matzui, M. I. Grybova, Y. I. Prylutskyy, U. Ritter, P. Scharff, Structure and magnetic properties of multi-walled carbon nanotubes modified with iron, Low Temp. Phys. 36 (2010) 1086-1090.

[16] U. Ritter, P. Scharff, G. E. Grechnev, V. A. Desnenko, A. V. Fedorchenko, A. S. Panfilov, Y. I. Prylutskyy, Y. A. Kolesnichenko, Structure and magnetic properties of multi-walled carbon nanotubes modified with cobalt, Carbon 49 (2011) 4443-4448.

[17] Q. Zhang, Q. J Jiao, Z. L Xuan, T. P Li, W. B. Yu, Preparation of carbon nanotube/expanded graphite composite material and its 8 mm wave attenuation properties, Acta Armamentarii 32 (2011) 1510-1513.

[18] J. J. Zhao, X. Xiao, I. Liu, Y. X. Guo, L. Yang, Effect of expanding volume of exfoliated graphite on millimeter-wave attenuation performance, Acta Photonica Sinica 43 (2014) 316003-316005.

[19] X. Ding, Y. Huang, S. Li, N. Zhang, J, Wang. $FeNi_3$ nanoalloy decorated on 3D architecture composite of reduced graphene oxide/molybdenum disulfide giving excellent electromagnetic wave absorption properties, J. Alloys Compd. 689 (2016) 208-217.

[20] C. Sun, K.N. Sun, P.F. Chui, Microwave absorption properties of Ce-substituted M-type barium ferrite, J. Magn. Mater. 324 (2012) 802-805.

[21] K. Chen, C. Xiang, L. Li, H. Qian, Q. Xiao, F. Xu, A novel ternary composite: fabrication, performance and application of expanded graphite/polyaniline/$CoFe_2O_4$ ferrite, J. Mater. Chem. 22 (2012) 6449-6455.

[22] P. Gairola, S. P. Gairola, V. Kumar, K. Singh, S. K. Dhawan, Barium ferrite and graphite integrated with polyaniline as effective shield against electromagnetic interference, Synthetic Met. 221 (2016) 326-331.

[23] J. Zhang, J. Fu, F. Li, E. Xie, D. Xue, N. J. Mellors, Y. Peng, $BaFe_{12}O_{19}$ single-particle-chain nanofibers: preparation, characterization, formation principle, and magnetization reversal

mechanism, ACS Nano 6 (2012) 2273-2280.

[24] A. Tadjarodi, H. Kerdari, M. Imani, $Ba_{0.69}Sr_{0.17}Cd_{0.07}Zn_{0.07}Fe_{12}O_{19}$ nanostrucutres/conducting polyaniline nanocomposites: synthesis, characterization and microwave absorption performance, J. Alloys Compd. 554 (2013) 284-292.

[25] I. Krupa, M. Prostredny, Z. Spitalsky, J. Krajci, M. Almaadeed, Electrically conductive composites based on an elastomeric matrix filled with expanded graphite as a potential oil sensing material, Smart Mater. Struct. 23 (2014) 12.

[26] T.K. Zhao, X.L. Ji, W.B. Jin, S.S. Guo, H.Y. Zhao, W.H. Yang, X.Q. Wang, C.Y. Xiong, A.L. Dang, H. Li, T.H. Li, S.M. Shang, Z.F. Zhou, Electromagnetic wave absorbing properties of aligned amorphous carbon nanotube/$BaFe_{12}O_{19}$ nanorod composite, J. Alloys Compd. 703 (2017) 424-430.

[27] K. Hayashida, Y. Matsuoka, Electromagnetic interference shielding properties of polymer-grafted carbon nanotube composites with high electrical resistance, Carbon 85 (2015) 363-371.

[28] S. R. Dhakate, N. Chauhan, S. Sharma, J. Tawale, S. Singh, P. D. Sahare, R. B. Mathur, An approach to produce single and double layer graphene from re-exfoliation of expanded graphite, Carbon 49 (2011) 1946-1954.

[29] A. Ohlan, K. Singh, A. Chandra, S. K. Dhawan, Microwave absorption behavior of core-shell structured poly (3, 4-ethylenedioxy thiophene)-barium ferrite nanocomposites, ACS Appl. Mater. Interfaces 2 (2010) 927-33.

[30] L.Vovchenko, L. Matzui, O. Brusylovets, V. Oliynyk, V. Launets, A. Shames, O. Yakovenko, N. Skoryk, Synthesis and properties of ferrite nanopowders for epoxy-barium hexaferrite-nanocarbon composites for microwave applications, Materialwiss. Werkst. (Mater. Sci. Eng. Technol.) 47 (2016) 139-148.

[31] A. H Elsayed, O. M. Hemeda, A. Tawfik, M. A. Hamad, Remarkable magnetic enhancement of type-M hexaferrite of barium in polystyrene polymer, AIP Adv. 5 (2015) 107131.

[32] D. C. Marcano, D. V. Kosynkin, J. M. Berlin, A. Sinitskii, Z. Sun, A. Slesarev, L. B. Alemany, W. Lu, J. M. Tour, Improved synthesis of graphene oxide, ACS Nano 4 (2010) 4806-4814.

[33] J. Zhang, J. Fu, F. Li, E. Xie, D. Xue, N. J. Mellors, P. Yong, $BaFe_{12}O_{19}$ single-particle-chain

nanofibers: preparation, characterization, formation principle, and magnetization reversal mechanism, ACS Nano 6 (2012) 2273-2277.

[34] L, Li, K. Chen, H. Liu, G. Tong, H. Qian, B. Hao, Attractive microwave-absorbing properties of M-$BaFe_{12}O_{19}$ ferrite, J. Alloys Compd. 557 (2013) 11-17.

[35] W. W. Focke, H. Badenhorst, S. Ramjee, H. J. Kruger, R. V. Schalkwyk, B. Rand, Graphite foam from pitch and expandable graphite, Carbon 73 (2013) 41-50.

[36] M. Mishra, A. P. Singh, S. K. Dhawan, Expanded graphite-nanoferrite-fly ash composites for shielding of electromagnetic pollution, J. Alloys Compd. 557 (2013) 244-251.

[37] H. Shen, X. Q. Shen, M. Li, H. B. Liu, Z. Wang, Microwave absorption of double-layer absorber based on nanocomposite $BaFe_{12}O_{19}$/α-Fe and nanocrystalline alloy $Fe_{0.2}(Co_{0.2}Ni_{0.8})_{0.8}$ microfibers, Adv. Mater. Res. 1035 (2014) 339-343.

[38] R. Saito, M. Hofmann, G. Dresselhaus, A. Jorio, M. S. Dresselhaus, Raman spectroscopy of graphene and carbon nanotubes, Adv. Phys. 60 (2011) 413-550.

[39] M. Zhou, T. Tian, X. Li, X. Sun, J. Zhang, P. Cui, J. Tang, L. C. Qin, Production of graphene by liquid-phase exfoliation of intercalated graphite, Int. J. Electrochem. Sci. 9 (2014) 810-820.

[40] U. Ritter, P. Scharff, O. P. Dmytrenko, N. P. Kulish, Y. I. Prylutskyy, N. M. Belyi, V. A. Gubanov, L. A. Komarova, S. V. Lizunova, V. V. Shlapatskaya, Radiation damage and Raman vibrational modes of single-walled carbon nanotubes, Chem. Phys. Lett. 447 (2007) 252-256.

[41] C. He, S. Wu, N. Zhao, C. Shi, E. Liu, J. Li, Carbon-encapsulated Fe_3O_4 nanoparticles as a high-rate lithium ion battery anode material, ACS Nano 7 (2013) 4459-4469.

[42] O. S. Yakovenko, L. Y. Matzui, L L. Vovchenko, A. V. Trukhanov, I. S. Kazakevich, S. V. Trukhanov, Y. I. Prylutskyy, U. Ritter, Magnetic anisotropy of the graphite nanoplatelet-epoxy and MWCNT-epoxy composites with aligned barium ferrite filler, J. Mater. Sci. 1 (2017) 1-14.

[43] H. Chen, M. R. Golder, F. Wang, R. Jasti, A. K. Swan, Raman spectroscopy of carbon nanohoops, Carbon 67 (2014) 203-213.

[44] Y. Liu, F. F. Min, T. Qiu, J. B. Zhu, M. X. Zhang, Effect of the grain size on magnetic properties of nanocrystalline $CoFe_2O_4$ ferrite, Adv. Mater. Res. 308 (2011) 685-688.

[45] L. Kong, X. Yin, Y. Zhang, X. Yuan, Q. Li, F. Ye, L. Cheng, L. Zhang, Electromagnetic

wave absorption properties of reduced graphene oxide modified by maghemite colloidal nanoparticle clusters, J. Phys. Chem. C 117 (2016) 19701-19711.

[46] J. Gan, Q. Q. Ni, T. Natsuki, Electromagnetic wave absorption properties of barium titanate/carbon nanotube hybrid nanocomposites, J. Alloys Compd. 615 (2014) 84-90.

[47] A. Ameli, M. Nofar, C. Park, P. Potschke, G. Rizvi, Polypropylene/carbon nanotube nano/microcellular structures with high dielectric permittivity, low dielectric loss, and low percolation threshold, Carbon 71 (2014) 206-217.

[48] C. J. Li, B. N. Huang, J. N. Wang, Effect of aluminum substitution on microstructure and magnetic properties of electrospun $BaFe_{12}O_{19}$ nanofibers, J. Mater. Sci. 48 (2013) 1702-1710.

[49] A. Ghasemi, Remarkable influence of carbon nanotubes on microwave absorption characteristics of strontium ferrite/CNT nanocomposites, J. Magn. Magn. Mater. 323 (2011) 3133-3137.

[50] X. Zhou, Y H. Han, J. Zhou, L. Shen, P. R. Matli, J. Lee, S I. Bae, D. Y. Lee, Q. Huang, Ferrite multiphase/carbon nanotube composites sintered by microwave sintering and spark plasma sintering, J. Ceram. Soc. Jpn. 122 (2014) 881-885.

[51] X. Sun, J. He, G. Li, J. Tang, T. Wang, Y. Guo, H. Xue, Laminated magnetic graphene with enhanced electromagnetic wave absorption properties, J. Mater. Chem. C 1 (2012) 765-777.

[52] S. C. Chiu, H. C. Yu, Y. Y. Li, High electromagnetic wave absorption performance of silicon carbide nanowires in the gigahertz range, J. Phys. Chem. C 114 (2010) 1947-1952.

[53] X. B. Wang, W. F, Zhu, X. Wei, Y. X. Zhang, H. H. Chen, Preparation and millimeter wave attenuation properties of $NiFe_2O_4$/expanded graphite composites by low-temperature combustion synthesis, Mat. Sci. Eng. B 185 (2014) 1-6.

[54] S. Sutradhar, K. Mukhopadhyay, S. Pati, S. Das, D. Das, P. K. Chakrabarti. Modulated magnetic property, enhanced microwave absorption and Mössbauer spectroscopy of $Ni_{0.40}Zn_{0.40}Cu_{0.20}Fe_2O_4$ nanoparticles embedded in carbon nanotubes, J. Alloys Compd. 576 (2013) 126-133.

[55] X. Ren, H. Fan, Y. Cheng, Microwave absorption properties of double-layer absorber based on carbonyl iron/barium hexaferrite composites, Appl. Phys. A 122 (2016) 1-7.

[56] W. L. Song, X. T. Guan, L. Z. Fan, Y. B. Zhao, W. Q. Cao, C. Y. Wang, M. S. Cao, Strong and thermostable polymeric graphene/silica textile for lightweight practical microwave

absorption composites, Carbon 100 (2016) 109-117.

[57] N. Yousefi, X. Sun, X. Lin, X. Shen, J. Jia, B. Zhang, B. Tang, M. Chan, J. K. Kim, Highly aligned graphene/polymer nanocomposites with excellent dielectric properties for high-performance electromagnetic interference shielding, Adv. Mater. 26 (2014) 5480-5487.

[58] Y. Ding, Z. Zhang, B. Luo, Q. Liao, S. Liu, Y. Liu, Y. Zhang, Investigation on the broadband electromagnetic wave absorption properties and mechanism of Co_3O_4-nanosheets/reduced-graphene-oxide composite, Nano Res. 5 (2016) 1-11.

- A sandwich microstructured EG/BF prepared by *in-situ* sol-gel auto-combustion.
- The sandwich microstructured CNT/EG/BF improves electromagnetic performance.
- The bandwidth (< -10 dB) of CNT/EG/BF was up to 4.2 GHz in 2-18 GHz.